Biochimica et Biophysica Acta 1808 (2011) 1753–1763

Contents lists available at ScienceDirect

Biochimica et Biophysica Acta

journal homepage: www.elsevier.com/locate/bbamem

Interactions of the AT_1 antagonist valsartan with dipalmitoyl-phosphatidylcholine bilayers

C. Potamitis [a,b], P. Chatzigeorgiou [b], E. Siapi [a], K. Viras [b], T. Mavromoustakos [a,b,*], A. Hodzic [c,d], G. Pabst [c], F. Cacho-Nerin [c], P. Laggner [c], M. Rappolt [c,**]

[a] Institute of Organic and Pharmaceutical Chemistry, National Hellenic Research Foundation, Vas. Constantinou 48, Athens 11635, Greece
[b] Chemistry Department, National and Kapodistrian University of Athens, Panepistimiopolis Zographou 15771, Greece
[c] Institute of Biophysics and Nanosystems Research (IBN), Austrian Academy of Sciences, 8042 Graz, Austria
[d] Research Center Pharmaceutical Engineering GmbH, 8010 Graz, Austria

ARTICLE INFO

Article history:
Received 22 December 2010
Received in revised form 30 January 2011
Accepted 1 February 2011
Available online 18 February 2011

Keywords:
Valsartan
Dipalmitoyl-phosphatidylcholine
Bilayer
Small-angle and wide-angle X-ray scattering
Raman spectroscopy
Differential scanning calorimetry

ABSTRACT

Valsartan is a marketed drug with high affinity to the type 1 angiotensin (AT_1) receptor. It has been reported that AT_1 antagonists may reach the receptor site by diffusion through the plasma membrane. For this reason we have applied a combination of differential scanning calorimetry (DSC), Raman spectroscopy and small and wide angle X-ray scattering (SAXS and WAXS) to investigate the interactions of valsartan with the model membrane of dipalmitoyl-phosphatidylcholine (DPPC). Hence, the thermal, dynamic and structural effects in bulk as well as local dynamic properties in the bilayers were studied with different valsartan concentrations ranging from 0 to 20 mol%. The DSC experimental results showed that valsartan causes a lowering and broadening of the phase transition. A splitting of the main transition is observed at high drug concentrations. In addition, valsartan causes an increase in enthalpy change of the main transition, which can be related to the induction of interdigitation of the lipid bilayers in the gel phase. Raman spectroscopy revealed distinct interactions between valsartan with the lipid interface localizing it in the polar head group region and in the upper part of the hydrophobic core. This localization of the drug molecule in the lipid bilayers supports the interdigitation view. SAXS measurements confirm a monotonous bilayer thinning in the fluid phase, associated with a steady increase of the root mean square fluctuation of the bilayers as the valsartan concentration is increased. At high drug concentrations these fluctuations are mainly governed by the electrostatic repulsion of neighboring membranes. Finally, valsartans' complex thermal and structural effects on DPPC bilayers are illustrated and discussed on a molecular level.

1. Introduction

The renin–angiotensin system (RAS) is a bioenzymatic cascade [1] well known to influence the aldosterone stimulation and water homeostasis. When the amount of blood decreases in a human body, the kidneys start to secrete renin, which in turn stimulates the production of angiotensin I (Ang I). Ang I is then converted to angiotensin II (Ang II) by the angiotensin-converting enzyme (ACE). Finally, Ang II binds at the type 1 angiotensin (AT_1) receptor [2], and causes blood vessels to constrict resulting in an elevated blood pressure. Thus, the RAS has received great attention in developing novel synthetic antihypertensive drugs.

The first drug design strategy was to block ACE and subsequently the formation of the vasoconstrictive hormone Ang II. Captopril® was the first ACE inhibitor developed [3] and was considered a major breakthrough, because of its novel mechanism of action. However, ACE inhibitors have undesired side effects such as dry mouth and angioedema, which precluded them from being the ideal drugs for hypertension. Secondly, it is well known that also other non-ACE enzymatic pathways for the formation of Ang II exist [4], so that the inhibition of the RAS by ACE inhibitors is incomplete. A similar strategy is followed in the rational drug design of renin inhibitors. Only recently, the synthetic molecule aliskiren, which blocks the renin activity, has entered the market with the trade name Tekturna® (Novartis) [5].

The second strategy to reduce RAS activity focuses on a class of synthetic molecules that block the AT_1 receptor, i.e., they function as Ang II antagonists. Synthetic peptide analogs and other non-peptide Ang II antagonists are designed to mimic the C-terminal segment of Ang II [6]. In this class of antihypertension drugs losartan was the first

* Correspondence to: T. Mavromoustakos, Institute of Organic and Pharmaceutical Chemistry, National Hellenic Research Foundation, Vas. Constantinou 48, Athens 11635, Greece. Tel.: +30 2107274475; fax: +30 2107274261.
** Correspondence to: M. Rappolt, Institute of Biophysics and Nanosystems Research, Austrian Academy of Science, 8042 Graz, Austria. Tel.: +39 040 375 8708; fax: +39 040 375 8029.
E-mail addresses: tmavrom@chem.uoa.gr (T. Mavromoustakos), michael.rappolt@elettra.trieste.it (M. Rappolt).

0005-2736/$ – see front matter © 2011 Elsevier B.V. All rights reserved.
doi:10.1016/j.bbamem.2011.02.002

successful peptidomimetic analog to be marketed [4,7]. These angiotensin receptor blockers (ARBs) have been especially developed to produce a more effective inhibition of the action of Ang II as compared to other drug classes as well as to decrease the side effects [8–16].

Valsartan (Diovan®) is the second orally active non-peptide Ang II antagonist marketed in Europe and the USA for the treatment of hypertension. Its effectiveness is at least equivalent to ACE inhibitors, diuretics, β-blockers and calcium antagonists, and it has the advantage of not causing cough and lower limb edema such as ACE inhibitors do [17–19]. Valsartan differs structurally from losartan by an alkylated aminoacid that replaces the heterocyclic moiety of the compound. Like losartan, its rational design is based on the mimicry of the C-terminal segment of Ang II (Fig. 1, red circle) [20,21].

Recently, we have reported that losartan and subsequently also other ARBs may exert their mode of action through a two-step mechanism, which involves membrane incorporation and lateral diffusion towards the receptor site, rather than a direct drug–receptor interaction [22,23]. A two-step mechanism has been also suggested for other amphiphilic molecules such as cannabinoids and calcium channel antagonists [24–26].

In order to profoundly examine the role of the lipid bilayers, the interaction of valsartan with a simple model membrane system was studied. Usually, phosphatidylcholine (PC)–water or PC–cholesterol–water systems are applied to mimic plasma cell membranes. In this work, multilamellar vesicles (MLVs) of dipalmitoyl-phosphatidylcholine (DPPC) formed in excess of water were used to model the plasma membranes of the vasculature. Note that AT_1 receptors are found in many tissues [1], but primarily in the plasma membranes of the blood vessel system, where ARB's attachment to the receptors causes a decrease in vasoconstriction [27]. Further, note that saturated PCs are the most abundant lipid species in the plasma membrane of the vasculature with a share 40–65% [28,29]. Conveniently, the thermodynamic and structural properties of DPPC have been extensively studied [30–35].

The main focus of this study are valsartan–lipid interactions observed in a temperature range from 20 up to 50 °C, i.e., in the gel and fluid phases of DPPC bilayers. Both, the pre- and main transitions have been characterized by Differential Scanning Calorimetry (DSC), Raman spectroscopy, small and wide angle X-ray scattering (SAXS and WAXS), and dilatometry experiments (only at 50 °C). These methodologies provide insight into the thermodynamic changes in the membrane in the presence of valsartan, allow the determination of chain fluidity and mobility alterations, and finally permit to correlate the spectroscopic results with the structural modifications on a molecular level. Moreover, the swelling behavior of the MLVs helps to understand the role of charged valsartan molecules. A realistic bilayer model for partial interdigitation is presented, and the complex thermal valsartan–lipid behavior is discussed.

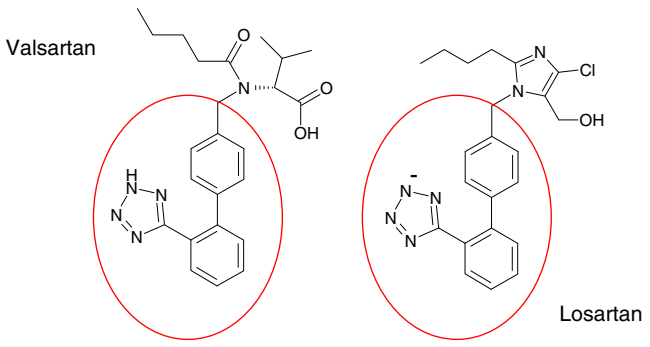

Fig. 1. Chemical structures of valsartan and losartan. The molecular part mimicking the C-terminal segment of angiotensin II is circled in red.

2. Materials and methods

2.1. Sample preparation

L$_\alpha$-dipalmitoyl-phosphatidylcholine (L$_\alpha$-DPPC, 99 + %) was purchased from Avanti Polar Lipids Inc (Alabaster, AL) and spectroscopic grade $CHCl_3$ from Sigma Aldrich (St. Louis, MO). Valsartan was generously donated by Novartis. For DSC and Raman measurements, appropriate amounts of DPPC and valsartan diluted in chloroform were mixed, dried under a stream of N_2 and then stored under vacuum overnight. After dispersing in water (50% w/w), ca. 5 mg were sealed in stainless steel capsules obtained from Perkin-Elmer (Norwalk, CT) and used for differential scanning calorimetry, and 40 mg were positioned in the sample holder for Raman spectroscopy measurements. For X-ray scattering experiments MLVs were prepared according to the above protocol with final lipid weight concentrations of 5% and 20%. The drug concentrations used for the different experiments were $x = 0.01$ (1 mol% valsartan), $x = 0.02$, $x = 0.05$, $x = 0.10$ and $x = 0.20$.

2.2. Differential scanning calorimetry

Thermal scans were carried out using a Perkin-Elmer DSC-7 calorimeter (Norwalk, CT). All samples were scanned from 10 to 60 °C until identical thermograms were obtained using a scanning rate of 2.5 °C/min. The temperature scale of the calorimeter was calibrated using indium ($T_m = 156.6$ °C) and DPPC bilayers ($T_m = 41.2$ °C). The following diagnostic parameters were used for the study of drug to membrane interactions: T_m (maximum of the recorded heat capacity), T_{onset} (the starting temperature of the phase transition) and ΔT (the full width at half-height of the phase transition), and the respective parameters concerning the pretransition. An empty pan for the base line and a sample containing double-distilled water were run for the temperature range of 10–60 °C as a reference for the background. This background was subtracted from each thermal scan of the samples. The area under the peak represents the enthalpy change during the transition (ΔH). The mean values of ΔH of three identical scans were tabulated.

2.3. Raman spectroscopy

The Raman spectra were obtained from 3500 to 400 cm^{-1} with 4 cm^{-1} spectral resolution using a Perkin-Elmer NIR FT-spectrometer (Spectrum GX II, Norwalk, CT) equipped with CCD detector (Norwalk, CT). The measurements were performed at a temperature range of 27–50 °C. The laser power (near IR-Nd:YAG laser with a wavelength of 1064 nm, Norwalk, CT) was controlled to be constant within 400 mW during the experiments. 1500 scans were accumulated and back scattering light was collected.

2.4. Small and wide angle X-ray scattering

Simultaneous small and wide-angle X-ray scattering (SAXS and WAXS = SWAXS) experiments were carried out at the Austrian SAXS beamline (Elettra Laboratory, Sincrotrone Trieste, Italy) [36]. Two linear one-dimensional gas detectors were used covering the q ranges ($q = 4\pi \sin\theta/\lambda$; where 2θ is the scattering angle and $\lambda = 1.54$ Å the selected X-ray wavelength) between 0.01 and 0.6 $Å^{-1}$ for SAXS and from 0.67 to 1.95 $Å^{-1}$ for WAXS, respectively. The angular dependence of the scattered intensity was calibrated with silver behenate ($d = 58.38$ Å) for the SAXS regime, and with para-bromo benzoic acid for the WAXS regime. The instrumental resolution was determined to have a full width at half maximum of $\Delta q = 2.23\ 10^{-3}$ $Å^{-1}$. The lipid dispersions were measured in quartz glass capillaries (diameter 1 mm) and thermostated in a custom-built sample holder block of brass, which was connected to a circulating water bath (Unistat CC,

Huber, Offenburg, Germany). For static measurements the sample was equilibrated before exposure for a period of 10 min. Exposure times were 2–3 min. Background corrected SAXS patterns were analyzed in the full q-range allowing the application of the paracrystalline ansatz for lattice disorder (used for the gel-phase fitting) as well as of the modified Caillé theory (used for the fluid phase fitting). The technique and underlying premises have been described previously in detail [37,38] and for reviews, see ref. [34,39]. The bilayer model used and its applications have been recently presented [40]. From the fits to the scattered intensities $I = S(q)|F(q)|^2/q^2$ ($S(q)$: structure factor; $F(q)$: form factor) we directly obtained the lamellar repeat distance d and the head group-to-head group thickness d_{HH}. The width σ_H of the Gaussian peak applied to model electron density profile of the head group region was fixed to 3 Å. Note that steric bilayer thicknesses are not explicitly discussed in this work, but can easily be obtained by e.g. applying the equation $d_B = d_{HH} + 4\sigma_H$ [38]. In the gel phase, the fluctuations of lamellar stacking disorder σ(gel) were determined from the paracrystalline structure factor. Fluctuations of the interstitial water layer of fluid bilayers were derived via the bending fluctuation or Caillé parameter,

$$\eta = \frac{\pi\, k_B T}{2d^2\sqrt{K_C B}} \tag{1}$$

directly from the fits. η depends on membrane bending rigidity K_C and the bulk modulus of interactions B. The mean square fluctuation in the water spacing between the bilayers was then obtained from $\sigma(\text{fluid})^2 = \eta\, d^2/\pi^2$ (for a review on bending fluctuations see [34]).

The lateral area per molecule in the fluid phase was determined from

$$A(x) = \frac{2\cdot V(x)}{d_{\text{Luzzati}}(x)} \approx \frac{2\cdot V(x)}{d_{HH}(x)}, \tag{2}$$

where V is the effective molecular volume (cf. to section 2.4) and d_{Luzzati} is the membrane thickness that is defined by the Gibbs dividing surface [41]. Note that for pure DPPC bilayers in the fluid phase d_{Luzzati} has nearly the same value as d_{HH} [42]. The influence of insertion of valsartan into the bilayers onto the Gibbs dividing surface was not considered. In the case of a linear dependence of $A(x)$ one can extract estimates for the partial molecular areas A_{DPPC} and A_{val} by the relation [43]:

$$A(x) = x\, A_{val} + (1-x)\cdot A_{DPPC}. \tag{3}$$

2.4. Dilatometry

The density ρ of the liposomal dispersions has been determined using a DSA 5000 density analyzer (Anton Paar, Graz, Austria). Further experimental details are described in [44]. From the density data the apparent specific partial lipid volumes were calculated using the relation

$$\varphi_V = 1/\rho_o\cdot[1-(\rho-\rho_o)/c], \tag{4}$$

where ρ is the measured density of the solution, ρ_o is the density of the solvent (0.988 g/cm^3) and c is the solute concentration (5 mg/cm^3). The effective molecular volume V of the valsartan/DPPC mixtures were derived according to Greenwood et al. [45] by

$$V(x) = \frac{x\cdot M_{val} + (1-x)\cdot M_{DPPC}}{N_A}\cdot\varphi_V \tag{5}$$

where $M_{val} = 436$ and $M_{DPPC} = 734$ g/mol are the molecular weights of valsartan and DPPC, respectively, N_A is the Avogadro's number, and x is the valsartan fraction. Assuming that valsartan does not affect the molecular volume of DPPC, i.e., condense or expand, V can be estimated from

$$V(x) = x\, V_{val} + (1-x)\cdot V_{DPPC} \tag{6}$$

using $V_{val} = 597$ Å^3 (estimated from valsartan's density in the solid state $\rho = 1.20 \pm 0.02$ g/cm^3 [46] and its molecular weight) and value of $V_{DPPC} = 1228$ Å^3 [45].

3. Results

3.1. Differential scanning calorimetry

The recorded calorimetric scans from DPPC multilamellar vesicles in excess of water are presented in Fig. 2 for valsartan fractions of $x = 0$, 0.01, 0.05 and 0.20. For the $x = 0$ and 1 mol% samples two characteristic endothermic peaks are observed corresponding to the pre- and the main transition, respectively. Below pretransition temperature, T_{pre} , the lamellar gel phase, $L_{\beta'}$, is present, in which the lipid chains are in all-trans conformation [47], and as depicted schematically in Fig. 2 are tilted with respect to membrane normal about 32° [48]. Above the main transition temperature, T_m, the fluid lamellar phase, L_α, is apparent. An intermediate phase, $P_{\beta'}$, is observed in the temperature range from T_{pre} to T_m, in which the bilayers are modulated by a periodic ripple (ripple phase) [49]. The measured transition temperatures and enthalpies for the pure DPPC–water system are in good agreement with literature values [30] (Table 1). The presence of valsartan modulates the following thermal events. At only 1 mol% of the drug, the pretransition is almost suppressed, the enthalpy is lowered by a factor of three and the transition width spans over 7–8 °C. This clearly illustrates the interface activity of the drug molecule. Further, with increasing drug concentration, the main transition temperature and the transition cooperativity decrease monotonically. This demonstrates that valsartan affects increasingly the alkyl chain packing, when the concentration is increased. A closer look at the main transition for 5 and 20 mol% valsartan concentration, reveals a splitting of the transition into two components (Table 1: components I and II). The total enthalpy of the main transition increases quite significantly from 7.5 to 9.8 kcal/mol for $x = 0.01$–0.20. As we will discuss later this enthalpy increase indicates at least a partial interdigitation of the alkyl chains.

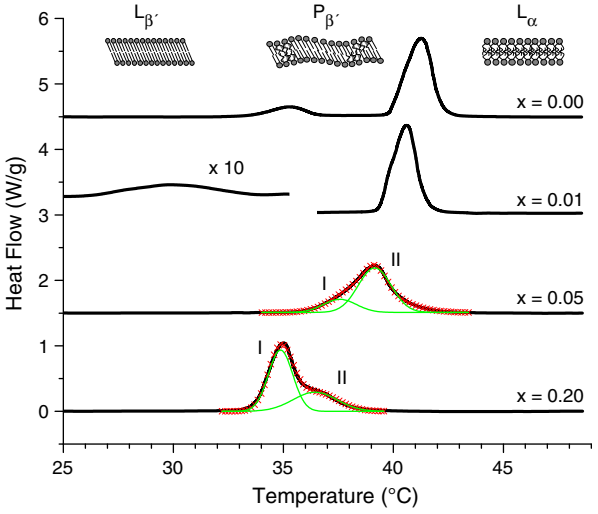

Fig. 2. DSC scans of DPPC bilayers containing valsartan at molar ratios $x = 0.00$, 0.01, 0.05 and 0.20. The thermal scan attributed to DPPC bilayers shows two distinct thermal events. The incorporation of the drug eliminates the small endothermic event (pretransition) for $x > 0.01$. The higher the incorporated concentration of the drug, the broader the transition width and the lower the phase transition temperature. At 5 and 20 mol% valsartan incorporation, the main transition splits into components (cp. Table 1).

Table 1
Thermodynamic parameters of pure DPPC bilayers and with valsartan (VAL) incorporated at molar ratios $x = 0.01$, 0.05 and 0.20. The pretransition as well as main transition parameters T_{pre}, ΔT_{pre} T_m, ΔT_m and ΔH are given.

Samples	T_{pre} (°C)	ΔT_{pre} (°C)	ΔH_{pre} (kcal/mol)	T_m (°C)	ΔT_m (°C)	ΔH_m (kcal/mol)
DPPC ($x = 0.0$)	35.2	1.8	1.12 ± 0.02	41.2	1.4	**7.35** $\pm$ 0.07
DPPC/VAL ($x = 0.01$)	29.8	4.7	0.38 ± 0.01	40.5	1.3	**7.53** $\pm$ 0.07
DPPC/VAL ($x = 0.05$)	–	–	–	I: 37.6 II: 39.2	1.8 1.8	$1.64 \pm 0.02 +$ $6.05 \pm 0.06 =$ **7.69** $\pm$ 0.07
DPPC/VAL ($x = 0.20$)	–	–	–	I: 34.9 II: 36.4	1.3 2.0	$6.25 \pm 0.06 +$ $3.54 \pm 0.03 =$ **9.80** $\pm$ 0.09

The table refers to experiments displayed in Fig. 2.

3.2. Raman spectroscopy

Raman spectra of pure DPPC bilayers and in the presence of $x = 0.20$ valsartan were obtained in a temperature range of 27–50 °C and were recorded in a range of 400–3500 cm^{-1}. The transition behavior was especially characterized by the C–C and C–H stretching modes. In particular the C–H stretching bands at ~2880 cm^{-1} and ~2850 cm^{-1} have been analyzed, which are assigned to symmetric and antisymmetric stretching modes in the methylene groups (CH_2), respectively, while the band at ~2935 cm^{-1} is correlated to the chain terminal methyl C-H symmetric stretching modes [50,51]. Further, spectral bands near 1100 cm^{-1} related to the C–C stretching modes [52] have been investigated (for a recent overview on Raman spectra of DPPC bilayers see ref. [53]).

The bands at ~1090 cm^{-1} and ~1130 cm^{-1} reflect the C–C stretching modes in *gauche* and *trans* conformation, respectively, i.e., intramolecular *trans-gauche* conformational changes within the hydrocarbon chain region can be monitored directly by the intensity ratio $I_{1090/1130}$. This peak height intensity ratio allows the direct comparison of the bilayers order–disorder transitions between liposome preparations without or with drug incorporation [54]. In Fig. 3 the changes in $I_{1090/1130}$ intensity ratio in pure DPPC as well as DPPC/valsartan bilayers are presented ($x = 0$ and 0.2). The transition temperatures compare well to the results found from the calorimetric measurements (Fig. 3A, B), and it is clearly seen that valsartan induces a lowering of the *gauche*/*trans* ratio across the gel to fluid phase transition: ΔI drops from 0.83 to about 0.54, which means a reduction of about 35%. As can be seen in Fig. 3C, valsartan induces in part already at low temperatures (25–35 °C) some chain disorder in the gel phase, the main differences, however, are apparent in the fluid phase. The presence of valsartan reduces *gauche* to *trans* isomerizations by about 15% at 50 °C.

The most intense bands in the Raman spectrum of lipid samples are given in the methylene C–H stretching mode region 2800–3100 cm^{-1}, which are commonly used to monitor changes in the lateral packing properties and mobility of the lipid chain in both gel and liquid crystalline bilayer systems [55]. In particular, the analysis of the symmetrical and antisymmetrical methylene stretching bands allows investigating the thermotropic phase behavior of lipids. Levin and co-workers were the first to introduce the intensity ratio of these two bands I_{2850}/I_{2880} as an order parameter [32]. This ratio describes the main changes occurring in the hydrocarbon chain region of the lipids. It is sensitive to subtle changes in conformational order from rotations, kinks, twists and bends of the lipid chains[56]. In Fig. 4A the order parameter is plotted for pure DPPC bilayers. As given for the above described $I_{1090/1130}$ ratio, also the $I_{2850/2880}$ parameter displays clearly the three different phase regions of $L_{\beta'}$, $P_{\beta'}$ and L_α. Moreover, the transition temperatures from the DSC results are well in accordance. Although the change of ΔI in the presence of valsartan

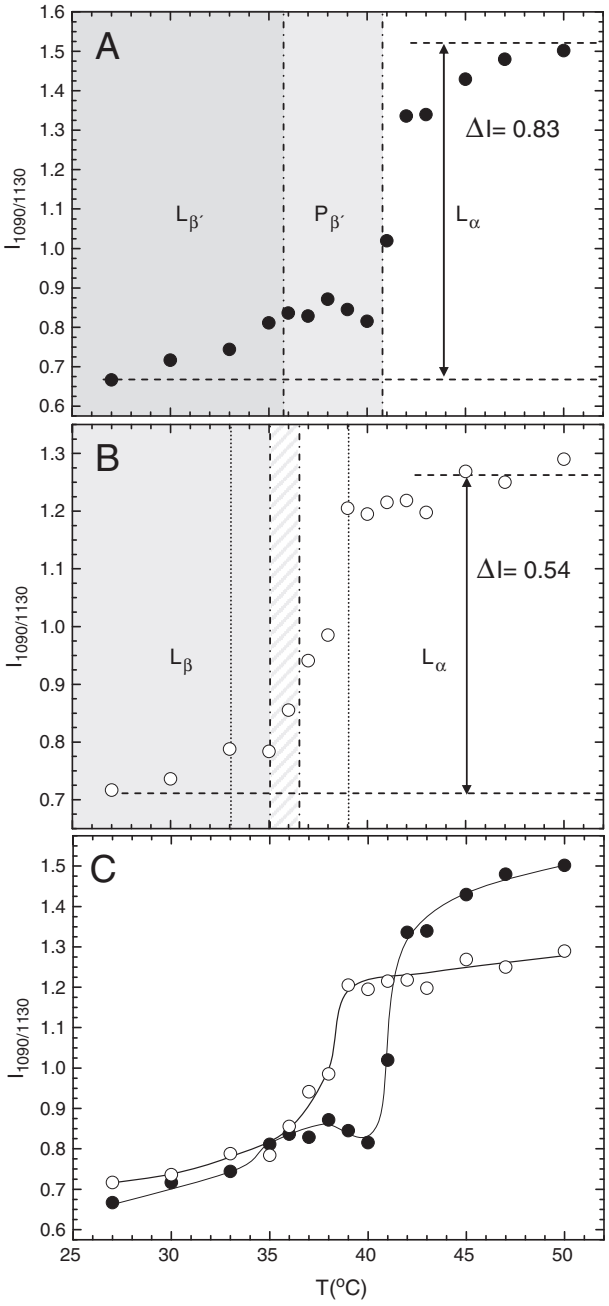

Fig. 3. $I_{1090/1130}$ vs. temperature plots for (A) pure DPPC (solid circles), (B) DPPC bilayers containing $x = 0.20$ of valsartan (open circles), and in superposition (C). DSC data have been included in first two panels by vertical lines: transition temperatures are identified with dashed-dotted lines and the complete transition-regime is marked by dotted lines (cp. Fig. 2).

is almost the same (Fig. 4B), the absolute values of I_{2850}/I_{2880} are clearly smaller in the pure gel and fluid phase regimes. As we will discuss later, this gives a clear indication for at least partial lipid interdigitation [57].

Another intensity ratio, namely $I_{2935/2880}$, measures effects originating from changes both in interchain and intrachain processes in the bilayer. Although the C–H stretching mode region consists of many superimposed vibrational transitions, the peak height intensity ratio is sensitive to monitor the lipid phase transitions [54,57,58]. However, the overall effect of valsartan on this parameter is not as remarkable as on the other two ratios discussed above. Nevertheless, the earlier onset of chain melting can be seen also here (inset of Fig. 4C).

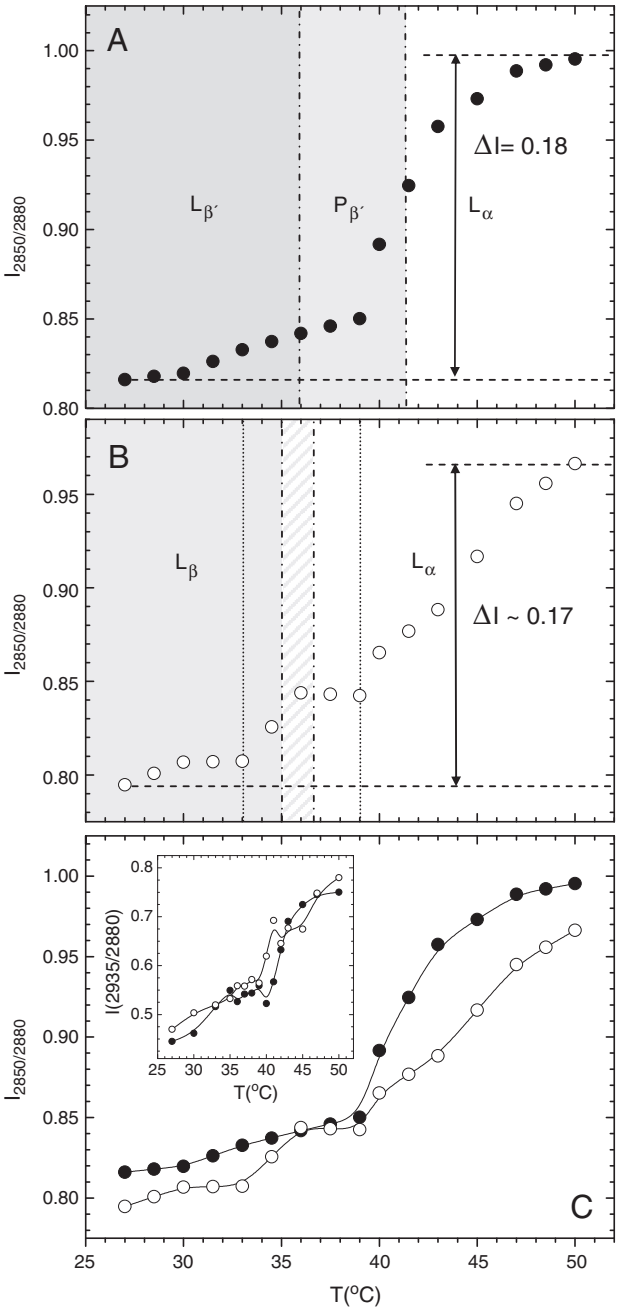

Fig. 4. $I_{2850/2880}$ vs. temperature plots for (A) pure DPPC (solid circle), (B) DPPC bilayers containing $x = 0.20$ of valsartan (open circles), and in superposition (C). DSC data have been included in first two panels by vertical lines: transition temperatures are identified with dashed-dotted lines and the complete transition-regime is marked by dotted lines (cp. Fig. 2). The inset illustrates the influence of valsartan on the $I_{2935/2880}$ ratio.

Other characteristic band alterations in the fluid phase provide evidence for the incorporation of valsartan in the monolayer leaflets of the DPPC membrane (data recorded at 43 °C). First, the band at 714 cm^{-1} which corresponds to C-N stretch vibrations, shows a shift to slightly higher wavenumbers, when valsartan is incorporated in lipid bilayers. Second, shift and line shape changes by valsartan at a band centered around 1720 cm^{-1} are observed. This indicates changes in the stretching vibrations of the C–O bonds, which are present in the ester groups of DPPC. Both observations prove that valsartan interacts with the PC head groups. Third, valsartan caused a shift of the 1296 cm^{-1} band to 1293 cm^{-1}, which corresponds to stretching vibrations in the $(CH)_2$ region of the acyl chains. Thus, direct evidence of valsartan interactions also with hydrophobic moieties of the DPPC bilayers is given.

3.3. X-ray scattering

Similar to the DSC scans, also simultaneous time-resolved SAXS and WAXS measurements were carried out on MLV dispersions. In the experiment from Fig. 5 the bilayers contained 5 mol% valsartan, and bilayer stacking as well as lipid chain packing were monitored in a temperature range from 20 to 50 °C with a temperature resolution of 1 °C per minute. In Fig. 5A the first two diffraction orders of the lamellar gel and fluid phase can be seen. In agreement with DSC results no signs for a ripple phase formation can be traced [59] (cp. Fig. 2). However, the lamellar repeat distance in the lamellar gel is anomalously high, i.e., from 20 to about 40 °C the d-spacing equals ~72 Å. Note that for the pure DPPC bilayer phase, the d-spacing lies around 64 Å (cp. Table 2). After the chain melting is completed, the L_α phase forms with a final d-value of about 67 Å. Interestingly, the intensities of the Bragg peaks in the fluid phase are significantly stronger than in the gel-phase, which means that the amount of spatially uncorrelated membranes is actually higher in the gel-phase as compared to the L_α phase. In this respect, it is also important to observe that the quasi long range order already improves significantly after the first main transition component at 37 °C is completed (indicated by the strong intensity increase of the diffraction peaks several degrees before the L_α phase forms; cp. Fig. 2, Table 1). Thus, a two-step transition is also reflected in the SAXS data. The chain order–disorder transition is measured by WAXS (Fig. 5B). The strong reflection at $q = 1.49$ $Å^{-1}$ arises from hexagonally packed chains and its intensity starts to decrease monotonically in the melting regime from 37 to 42 °C (Fig. 5C). In the L_α phase only diffuse scattering is apparent with a broad peak centered at about $q \sim 1.4$ $Å^{-1}$. The corresponding d-values are given in Fig. 5D, and show that in the gel-phase the nearest chain–chain distance continuously increases with temperature from 4.21 to 4.27 Å.

In Fig. 6 we take a closer look to the scattering patterns of DPPC bilayers in the presence of $x = 0.2$ valsartan at 20 and 50 °C, respectively. Again, we observe that valsartan induces stacking disorder in the MLVs, and that this disorder is stronger in the gel phase. In the bottom scattering pattern of Fig. 6A (20 °C), mainly form factor contributions are present accompanied only by a weak first order diffraction peak at $q = 0.08$ $Å^{-1}$. Both SAXS patterns have been analyzed by global fitting procedures [37], and best fits are displayed by solid red lines. The corresponding electron density profiles are displayed in Fig. 6B, and the most important structural parameters as well as the membrane fluctuation parameter σ are summarized in Table 2. Note that for the gel phase σ(gel) is deduced from the paracrystalline theory for lattice disorder of second type [60], i.e., practically flat bilayers are considered to oscillate with respect to the neighboring membranes, while for the fluid phase σ(fluid) is deduced from the application of the modified Caillé theory [61,62]. In the later theory also bilayer undulations are included. The most obvious alterations caused by valsartan are the loose stacking in the gel phase as evidenced by the large interstitial water layer ($\Delta(d - d_{HH}) = +27$ Å and $\Delta\sigma = +13$ Å; Table 2) and the enhanced diffuse scattering due to positionally uncorrelated membranes. The lipid chain packing area A_C at 20 °C was retrieved from the Bragg peak recorded at $q = 1.5$ $Å^{-1}$ (Fig. 6C), and is virtually the same as for pure DPPC bilayers (Table 2). This also holds true for the area per lipid, but only under the assumption of conserved chain tilt. In the fluid phase the bilayer swelling and increase of membrane fluctuation parameter are less pronounced ($\Delta(d - d_{HH}) = +5$ Å and $\Delta\sigma = +4$ Å; Table 2).

Finally, the influence of valsartan in the fluid phase at 50 °C was explored in a concentration range from $x = 0$ to 0.20. The key results from the SAXS experiments are given in the panels A–E of Fig. 7 and are complemented by the measured effective molecular volume V of

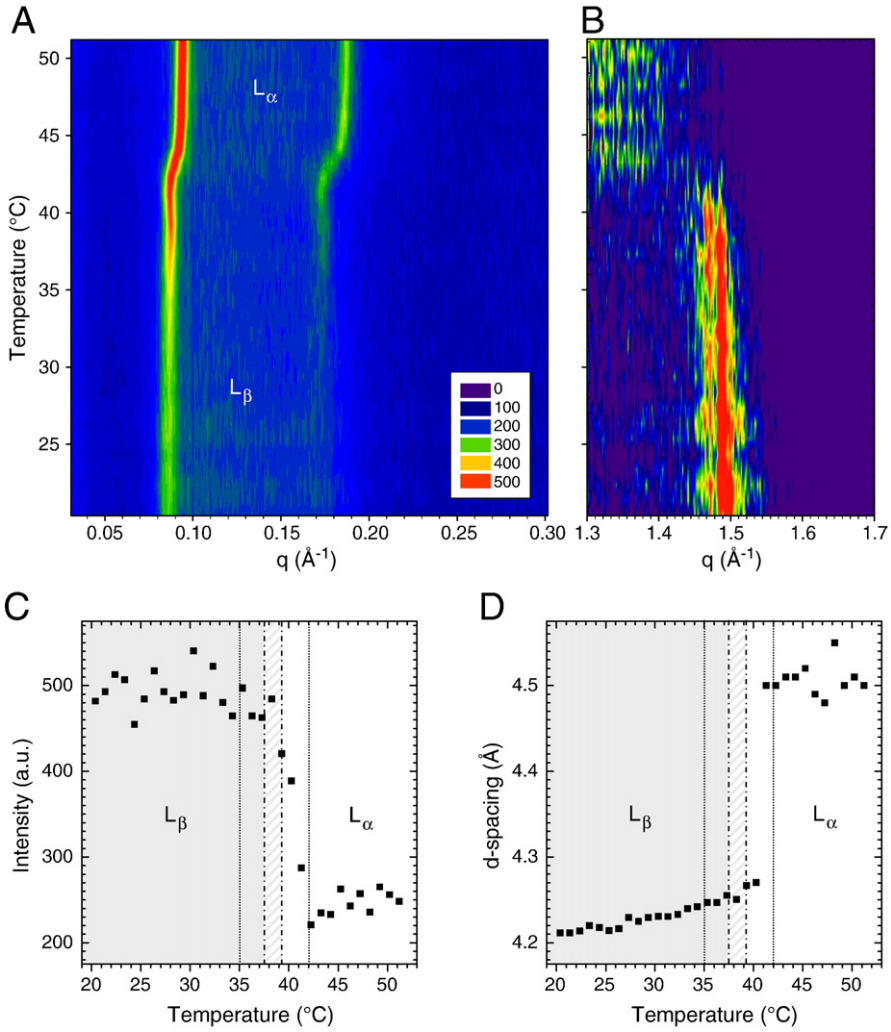

Fig. 5. Temperature scan experiment with DPPC/valsartan from 20 to 50 °C. The concentration of valsartan was 5 mol% and the scan rate was 1 °C/min. Structural changes during the main transition are observed simultaneously in the SAXS (A) and WAXS (B) regime. The contour plots demonstrate that the lamellar repeat distance decrease is accompanied by the loss of the chain order. In panel (C) the intensity drop of the WAXS peak at q~1.5 $Å^{-1}$ is shown, and as seen panel (D) the area/chain constantly increases already in the gel phase. For comparison, the DSC data have been included in the graphs C and D by vertical lines: transition temperatures are identified with dashed-dotted lines and the complete transition-regime is marked by dotted lines (cp. Fig. 2).

the valsartan/DPPC mixtures in panel F. Apart from the 2 mol% valsartan measurement, all other structural results follow monotonous trends as a function of the valsartan concentration. The induced membrane thinning from 38.3 to 34.8 Å (Δd_{HH}~3.5 Å; Fig. 7B) is accompanied by a steady increase in the mean fluctuation of the bilayers (Fig. 7C). Accordingly, the water spacing, $d - d_{HH}$ (Fig. 7D) increases continuously. Also the effective area per molecule, A, displays an almost linear behavior, if the 2 mol% valsartan measurement is neglected. This suggests that valsartan does not affect the lateral area of DPPC significantly and allows us to estimate the partial molecular areas for DPPC and valsartan applying Eq. (3) (solid line in Fig. 7E). A_{DPPC} results in 64 $Å^2 \pm 1$ $Å^2$ and $A_{valsartan} = 58 \pm 1$ $Å^2$. A_{DPPC} is well in agreement with literature data [42]. In Fig. 7F the behavior of the effective molecular volume of the studied DPPC/valsartan mixtures as a function of drug content is shown. A linear decrease of V is observed, similar to the previously reported volume reduction investigated for different sterol/PC mixtures [44]. However, unlike sterols, there is no condensation effect of valsartan on DPPC, because the weighted average of the bare molecular volumes fits the measured data fairly well (Eq. (6)). This agrees well with our observations on the lateral areas.

Table 2
Structural data on pure DPPC bilayers and DPPC with 20 mol% valsartan.

	DPPC (20 °C)	DPPC (50 °C)	DPPC/valsartan (20 °C)	DPPC/valsartan (50 °C)
d (Å)	63.5[a]	67.0[a]	86.3	68.8
d_{HH} (Å)	44.2[a]	38.3[a]	41	35
$d - d_{HH}$ (Å)	19.3[a]	28.7[a]	46	34
A (A_C) ($Å^2$)	47.9 (20.3)[a]	64[a]	48[d] (20.4)/–	64/58[e]
σ (Å)	1–2[b]	6[c]	14[b]	10

[a] Structural data taken from the review [42].
[b] Estimated values from global data analysis applying the paracrystalline theory.
[c] Data concerning the root mean square fluctuation in pure DPPC rely on data from [35,88].
[d] The partial area per lipid in the gel phase was calculated under the assumption of a chain conserved chain tilt.
[e] The partial areas A_{DPPC} and $A_{valsartan}$ were obtained by applying Eq. (3). Data refer to X-ray experiments of Fig. 6.

4. Discussion

4.1. Lipid conformational changes

Multilamellar vesicles of DPPC in excess of water undergo an endothermic melting transition, in which the hydrocarbon chains change from an all-*trans* conformation (gel phase) to a *trans-gauche*

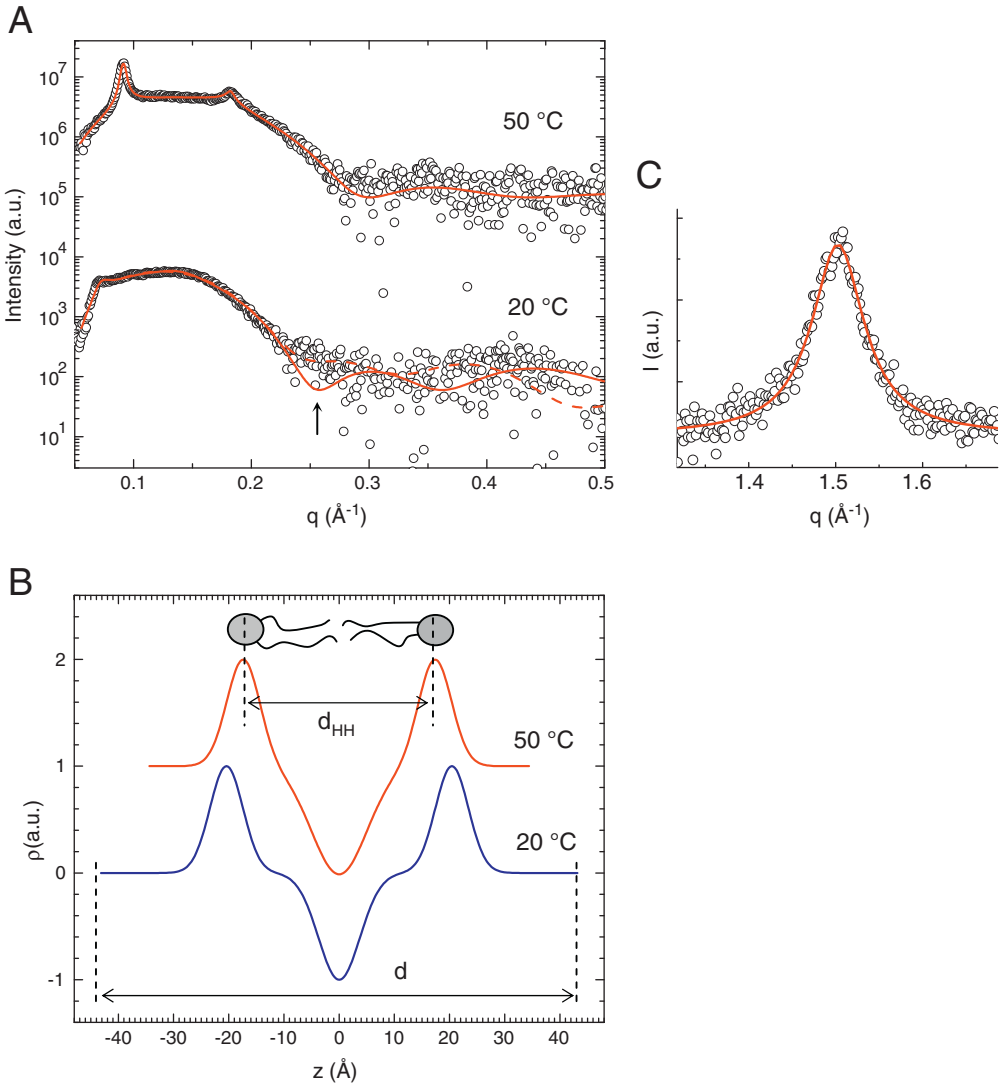

Fig. 6. X-ray scattering curves of DPPC/valsartan multilamellar vesicles at 20 °C and 50 °C (A), and their corresponding electron density profiles (B). In panel C the WAXS peak arising from the hexagonal chain packing is plotted. The full red lines in panels A and C give the best fit to the data. The most significant structural parameters are summarized in Table 2.

state (fluid phase). This is accompanied by a strong increase in the rotational mobility of both the lipid chains and the polar head group [30,35,63]. From dilatomeric and calorimetric experiments it is known that the main contributions to the excess of specific heat during this transition are due to volume expansion and *trans-gauche* isomerizations of the hydrocarbon chains. For DPPC bilayers, the van der Waals interaction energy accounts for 63% of the total enthalpy and changes in rotamer energy amount to 32% [64]. The number of induced *gauche* rotamers per DPPC molecule in the fluid phase has been estimated to be 5.6 [65]. The lipid conformation in the ripple phase is not fully understood yet. Several structural and dynamical studies [66–71] are consistent with the view that the ripple formation is related to the coexistence of alternating fluid- and gel-like domains [72], but alternative models describing the $P_{\beta'}$ phase built up by a single gel phase have also been put forward [73].

The incorporation of valsartan into the DPPC bilayers is expected to change at least in part the molecular packing and with it the conformational state of the lipids. The first indication for this notion is given by the DSC results (Fig. 2) demonstrating that already at 1 mol%, the pretransition is almost completely suppressed, a hint for its polar interface activity. Increasing the concentration of valsartan causes a lowering of T_m and a concomitant increase in ΔT (Table 1). This behavior is commonly found for many other membrane additives. Most prominent examples are given for PC-sterol interactions, in which the sterol incorporation renders on one hand the gel phase less solid, but on the other hand the L_α phase less fluid [74,75], and as a consequence reduces the cooperativity of the main transition (increase in ΔT). Direct evidence for this hypothesis is given by the Raman data in Fig. 3. Here, the C-C stretching mode ratios of the *gauche* to *trans* conformations are analyzed. The intensity ratio of these two bands (I_{1090}/I_{1130}) is sensitive to changes in the conformational acyl chain order [56]. Fig. 3A displays the transition of pure DPPC bilayers, which reproduces well the thermal events (cp. Fig. 2), and is in agreement with other published Raman data on DPPC bilayers [54,76]. Clearly, the situation is altered in the presence of 20 mol% of valsartan. The overall intensity ratio difference ΔI drops (Fig. 3B), and as shown in Fig. 3C, this is caused by a slight disturbance of the chain order in the gel phase, but is to the greatest part due to a reduction of the chain disorder in the fluid phase. Similar interaction behavior with DPPC bilayers have been reported recently for the novel synthetic pyrrolidinone analog MMK3 [23] as well as for losartan [76].

4.2. Altered lipid packing

Lipid chain conformation and lipid chain packing within the bilayer are strictly related, but are manifested in different

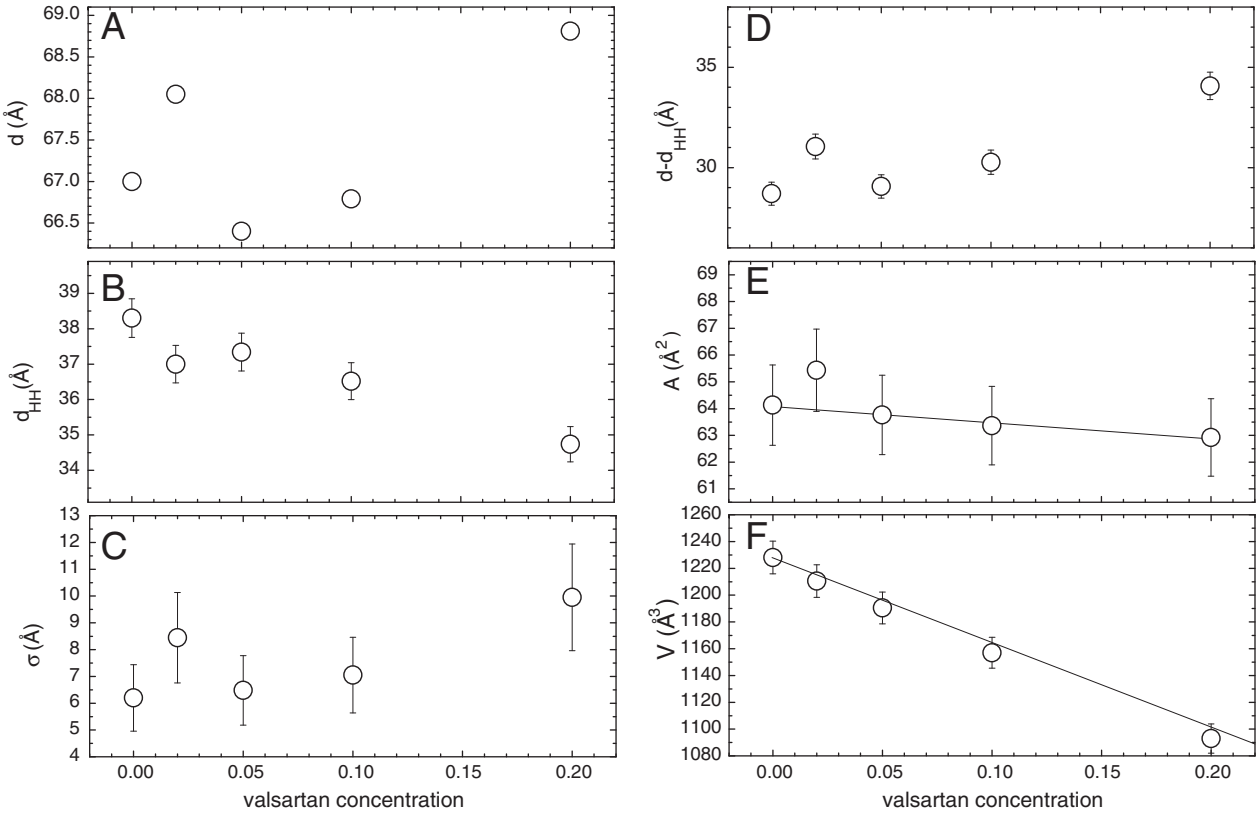

Fig. 7. Bilayer parameters as a function of valsartan concentration. A: *d*-spacing, B: head- to head group distance, d_{HH}, C: nearest neighbor distance fluctuations, σ, D: water layer thickness, d-d_{HH}, E: effective area per molecule, *A*, and F: effective volume per molecule, *V*. The straight line in panel E is the best fit to $A(x=0;0.05,0.1;0.2)$ using Eq. (3), and the straight line in panel F is an estimation of $V(x)$ applying Eq. (6).

experimental parameters. In this respect two important calorimetric findings are discussed. First, the total enthalpy of the main transition increases with the concentration of valsartan, i.e., from 7.4 to 9.8 kcal/mol (Table 1). Including also the enthalpic contributions of the pretransition this trend is slightly reversed for lower valsartan concentrations. Note that, for $x=0$, 0.01 and 0.05, $\Delta H_{pre}+\Delta H_m$ amounts to 8.5, 7.9 and 7.7 kcal/mol, respectively, but the overall enthalpy of 9.8 kcal/mol is clearly the greatest at 20 mol% valsartan content. Such an enthalpy increase of the main transition, especially at high drug concentrations, was also reported for DPPC-losartan interactions, where $\Delta H_m=9.1$ kcal/mol for $x=0.2$ [22]. The same behavior was found for dimyristoyl-PC-losartan interactions: an overall slight enthalpy decrease for drug concentrations from $x=0$ to 0.10 follows a monotonous enthalpy increase from $x=0.1$ to 0.5 [77]. This enthalpy trend at higher drug concentrations is somewhat unexpected, recalling that the change in the rotamer energy is reduced in the presence of valsartan, or in other words, less *trans-gauche* isomerizations of the hydrocarbon chains are expected during the turnover from the gel to the fluid state, which in principle means a reduction of the transition enthalpy. Consequently this means that valsartan most probably increases the van der Waals interaction contribution (other energetic contributions to the main transition such as hydrogen bonds account for less than 5% [64]). A possible explanation would be that above a certain critical drug concentration, valsartan not only constitutes a membrane impurity, but instead mediates chain interdigitation in the gel phase. For instance it was shown that for distearoyl-PC (in the presence of ethanol) the enthalpy of the interdigitated $L_{\beta I}$ to L_α phase transition is about 1 kcal/mol bigger as compared to the main transition of pure distearoyl-PC [78]. Second, this hypothesis would also deliver a possible explanation for the observation of the two component transition for $x\geq 0.05$ (cp. Fig. 2, Table 1). At this point it is speculative to assume that valsartan-rich domains inducing the interdigitated $L_{\beta I}$ phase coexist with valsartan-poor regions conserving mainly the $L_{\beta'}$ phase (Fig. 8A and B), but as will be outlined in the next two paragraphs, also the Raman and X-ray experiments are in line with this interpretation.

Levin and co-workers demonstrated that the intensity ratio I_{2850}/I_{2880} of the symmetric and asymmetric C–H stretching bands can be considered not only a general order parameter to monitor chain melting transitions, but also to sense different types of chain interdigitation [57,79]. For instance, perdeuterated glycerol induces chain interdigitation in DPPC bilayers, which is reflected in a decrease of the I_{2850}/I_{2880} ratio [57]. The effects of 20 mol% valsartan on DPPC bilayers are alike (Fig. 4). The transition temperatures from calorimetric measurements (Table 1) superimposed to the Raman data are in reasonable agreement, and furthermore the I_{2850}/I_{2880} ratio is slightly decreased in the temperature interval from 20 to 35 °C (Fig. 4C). Interestingly, the ratios are virtually the same from 36 to 40 °C. In agreement with Levin [57] the I_{2935}/I_{2880} is not sensitive to chain interdigitation (see inset Fig. 4C). Thus, two thermal regimes can be discerned in the gel phase, and following the train of thought of Levin, the interdigitated domains in the gel phase convert first (Fig. 4C). In the afore mentioned depiction, the transition component I (T_m *(I)* = 34.9 °C; Table 1) would hence be due to the chain melting of valsartan-rich domains in the $L_{\beta I}$ phase followed by the transition component II reflecting the chain melting of valsartan-poor domains, which remained predominately in the $L_{\beta'}$ phase (Table 1). Briefly, a $(L_{\beta I}+L_{\beta'})\rightarrow(L_\alpha+L_{\beta'})\rightarrow L_\alpha$ transition sequence is proposed.

This interpretation is also in agreement with X-ray data (Fig. 8). In the scattering pattern at 20 °C (Fig. 6A and C) two particularities should be noted. First, the shape of the diffraction peak in the wide angle range is perfectly symmetric, which implies a hexagonal chain packing, rather than a chain packing on an orthogonal lattice as found for pure DPPC bilayers [80,81]. Second, the simple bilayer model

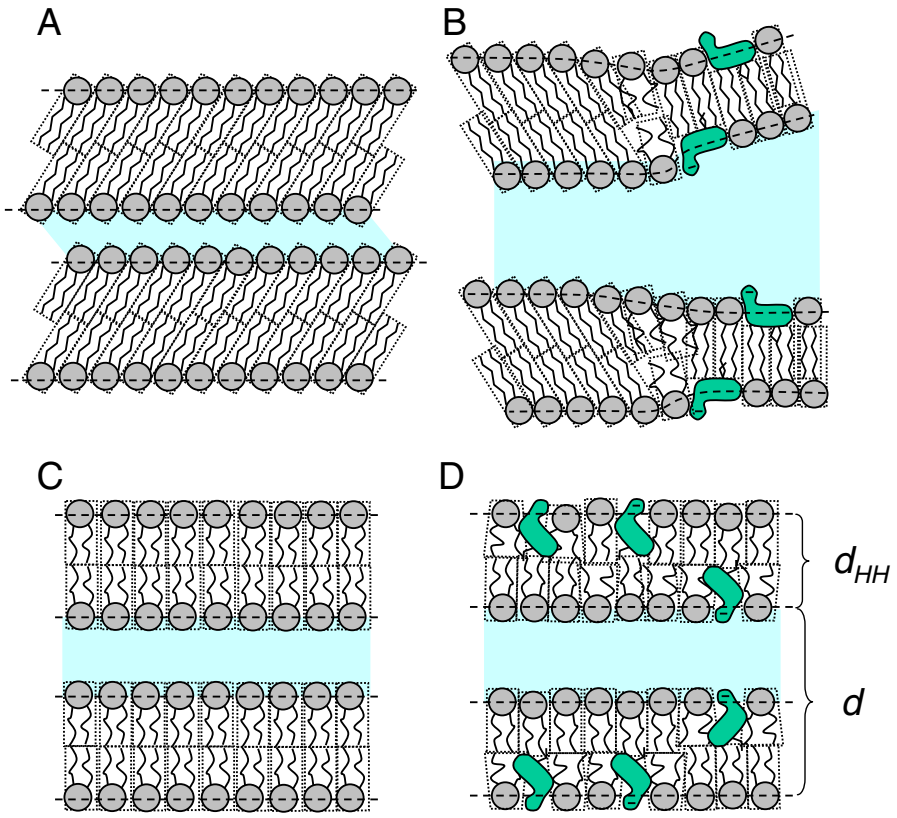

Fig. 8. Schematic illustration of DPPC bilayer structure alterations induced by valsartan. Without drug the $L_{\beta'}$ phase is present at 20 °C (A). The incorporation of 20 mol% valsartan induces the formation of valsartan-rich domains with chain interdigitation ($L_{\beta I}$ phase) and valsartan-poor domains which remain in the $L_{\beta'}$ phase (B). Panel C demonstrates pure DPPC bilayers in the L_α phase at 50 °C. The same conditions with 20 mol% valsartan are given in panel D. Dimensions in all panels base on the structural data given in Table 2.

commonly used in the global analysis routines [37] does not fit the SAXS pattern perfectly. At $q \sim 2.5$ Å^{-1} the best fit (solid red line) displays a first minimum of the form factor (see arrow), which is not seen in the scattering data. This deviation cannot be explained by the data scatter. Therefore, following the rationale of former studies [82,83], a combination of two form factor models was applied. One referring to a conserved bilayer structure ($L_{\beta'}$ phase as known from the pure DPPC system) and the other related to a bilayer with fully interdigitating non tilted chains ($L_{\beta I}$ phase). The bilayer thicknesses, d_{HH}, were determined to be about 45 and 32 Å, respectively, which comes very close to a conserved $L_{\beta'}$ [42] and a fully interdigitated $L_{\beta I}$ phase. The fraction of the $L_{\beta I}$ phase was a further fit parameter and turned out to be in the order of 75%, i.e., accordingly 25% of the sample remains in the $L_{\beta'}$ phase. This alternative model improved the fitting quality significantly (see dashed red line), however, the results have to be taken with due care. The assumed scenario is reasonable, but it is not the only possible one. For instance also partial interdigitation may occur, thus, how the lipids actually rearrange in the presence of valsartan cannot be ascertained, but most probably some amount of the lipids in the gel phase are interdigitated, because the measured form factor displays no clear first minima at $q = 2.5$ Å^{-1}. This finally means that all experimental data are in accordance with the illustration given in Fig. 8B.

Last, we would like to point out that a small percentage of lipids with molten chains are likely to coexist with lipids in all-*trans* conformation in order to smoothen borders between $L_{\beta I}$ and $L_{\beta'}$ phase domains. Similar ideas have been also proposed for the stable ripple phase of PCs [67,71,72].

In the fluid phase, the incorporation of 20 mol% of valsartan does not alter the bilayer structure as drastically. The data are satisfactorily fitted with the common bilayer model [37] (Figs. 6A and B, upper curves). Nevertheless, there is a pronounced thinning of the membrane thickness, d_{HH}, from 38.3 to 35 Å (Fig. 7B, Table 2), which might be explained by induced partial interdigitation (illustrated in Figs. 8C and D). In fact the partial lateral areas of valsartan are comparable to those of DPPC. Hence valsartan may partition into the membrane such that it basically replaces one DPPC molecule and shields the methyl terminus of the DPPC hydrocarbons in the opposing membrane leaflet. This further supports the hypothesis that the enthalpy increase of the main transition at high valsartan concentrations is mainly caused by an increase of the van der Waals energy contribution.

4.3. Bilayer swelling and stacking disorder

The equilibrium water layer thickness between adjacent bilayers is determined by the inter-membrane forces. For neutral (non-charged) membranes the attractive van der Waals force is balanced by the repulsive Helfrich undulation force. Other short range forces such as steric repulsion or hydration forces do not play any role in our study, because the inter-membrane distances are far too big (for a review see [84]). As can be seen in Figs. 8A and 8C (Table 2) the water layer thickness is usually bigger in the L_α than in the $L_{\beta'}$ phase. This is readily understood, because the bending rigidity of a fluid bilayer is smaller, which in turn causes an increased Helfrich repulsion force [34]. However, this is not the case for the DPPC/valsartan system. The opposite holds true, the water layer thickness is bigger in the gel phase as compared to the fluid phase (Figs. 8B and D; Table 2). Even more, the amount of correlated bilayers in the gel phase is smaller than in the L_α phase, which is visible to the naked eye in Fig. 6A: the first order Bragg-peak intensity is rather minute, tantamount to the fact that the pattern is mainly displaying diffuse form factor scattering arising from spatially uncorrelated bilayers. However, in the presence of valsartan also electrostatic repulsion between the membranes has

to be considered [85]. Valsartan has a relatively low pK_a value of 4.9 [86], which means that under the given experimental conditions (pH 5–6), most of the valsartan molecules are deprotonized at their tetrazole ring, i.e., they carry a negative charge (Fig. 1). This causes a negative charge density at the bilayer surfaces, and hence an additional repulsion between adjacent bilayers. The observed swelling of the lamellar stacking in the MLVs in the presence of valsartan is therefore governed by electrostatic forces. Note also, that the area per lipid, A, and the surface charge density are indirectly proportional, which means that the electrostatic repulsion decreases above T_m. Since the area per molecule increases by about 30% (Table 2, Fig. 7E), also the electrostatic force, f_e, should decrease, if the valsartan concentration in the bilayers remains the same. In other words, the swelling of the bilayers in the fluid phase is less pronounced, because the electrostatic repulsion is weaker. Please note that other effects like an altered valsartan partitioning in the fluid bilayers and/or different penetration depths of valsartan in the fluid bilayer would also alter the electrostatic force. Nevertheless, the additional electrostatic repulsion explains the relatively high membrane mean square fluctuations, σ, in the presence of valsartan (Table 2 and Fig. 7C). It is well known that positional membrane correlations are a function of the bilayer bending rigidity constant K_C, but also depend on the bulk compressibility modulus B (cp. Eq. (1)). B is governed by the interaction potential well and decreases with increasing electrostatic repulsion [34].

5. Conclusion

As documented in the results/discussion sections valsartan induces a wide range of alterations in the model membrane system of DPPC. The most striking changes are: (i) the suppression of the pretransition at low drug concentrations; (ii) the induction of a two component main transition at higher drug concentrations; (iii) the increase of *gauche* conformers in the lipid chains at ambient temperature and its relative reduction above T_m; (iv) the pronounced swelling of the lamellar stacking in the MLVs, especially strongly expressed in gel phase; and (v) the increase of the membrane fluctuation parameter in both phases. Notably all these observations are in accordance with the illustrations given in Fig. 8. Above a certain drug concentration threshold, in the case of valsartan $x \geq 0.05$, in part chain interdigitation is induced in the gel phase bilayers ($L_{\beta I}$ phase). With increasing temperature first domains in the $L_{\beta I}$ phase convert to the L_α phase, and 1–2 °C thereafter the rest of the gel phase turns over.

Of greater biological relevance, however, are the interactions of valsartan with the DPPC bilayers in the fluid state. Most importantly, valsartan is (i) well incorporated in the membrane interface (no experimental signs for detachment were found, since bilayer swelling and lattice disorder increase linearly with x), (ii) the common bilayer profile is conserved, but a clearly thinner membrane core is observed for high valsartan concentrations, which goes along with (iii) a lateral expansion of the apparent area per lipid. These are important structural alterations of the bilayer and the results are conform with the proposed two-step mechanism that the ARB's insertion in the lipid bilayer is followed by the lateral diffusion to the AT_1 binding site [13]. However, which role the observed structural membrane modifications play for valsartan's final accessibility to the AT_1 receptor remains unclear. Obviously different lipidic environments could further modulate the drugs potency. In this respect, the role of cholesterol and lipid diversity in plasma membranes might be significant [44,74,75,87], and are under investigation in our group.

Acknowlegments

We wish to acknowledge pharmaceutical company Novartis for the generous donation of bioactive compound valsartan.

References

[1] M. Paul, A.P. Mehr, R. Kreutz, Physiology of local renin–angiotensin systems, Physiol. Rev. 86 (2006) 747–803.
[2] M. De Gasparo, K.J. Catt, T. Inagami, J.W. Wright, Th. Unger, International Union of Pharmacology. XXIII. The angiotensin II receptors, Pharmacol. Rev. 52 (2000) 415–472.
[3] B. Rubin, M.J. Antonaccio, Z.P. Horovitz, Captopril (SQ 14, 225) (D-3-mercapto-2-methylpropanoyl-L-proline): a novel orally active inhibitor of angiotensin-converting enzyme and antihypertensive agent, Progr. Cardiovascular Diseases 21 (1978) 183–194.
[4] C.I. Johnston, Angiotensin receptor antogonists: focus on losartan, Lancet 346 (1995) 1403–1407.
[5] J.L. Pool, M. Azizi, M. Azizi, J.-C. Aldigier, A. Januszewicz, W. Zidek, Y. Chiang, Aliskiren, an orally effective renin inhibitor, provides sntihypertensive efficacy alone and in combination with valsartan, J. Am. Hypert. 20 (2007) 11–20.
[6] C. Sakarellos, K. Lintner, F. Piriou, S. Fermandjian, Conformation of the central sequence of angiotensin II and analogs, Biopolymers 22 (1983) 663–687.
[7] P.C. Wong, T.B. Barnes, A.T. Chiu, D.D. Christ, J.V. Duncia, W.F. Herblin, P.B.M.W.M. Timmermans, Losartan (DuP 753), an orally active nonpeptide angiotensin II receptor antagonist, Cardiovasc. Drug Rev. 9 (1991) 317–339.
[8] I. Martin, J.M. Ruysschaert, Common properties of fusion peptides from diverse systems, Biosci. Rep. 20 (2000) 483–500.
[9] E.L. Schiffrin, Vascular and cardiac benefits of angiotensin receptor blockers, Am. J. Med. 113 (2002) 409–418.
[10] L.M. Ruilope, E.A. Rosei, G.L. Bakris, G. Mancia, N.R. Poulter, S. Taddei, T. Unger, M. Volpe, B. Waeber, F. Zannad, Angiotensin receptor blockers: therapeutic targets and cardiovascular protection, Blood Press. 14 (2005) 196–209.
[11] G. Reboldi, F. Angeli, C. Cavallini, G. Gentile, G. Mancia, P. Verdecchia, Comparison between angiotensin-converting enzyme inhibitors and angiotensin receptor blockers on the risk of myocardial infarction, stroke and death: a meta-analysis, J. Hypertens. 26 (2008) 1282–1289.
[12] T. Mavromoustakos, A. Kolocouris, M. Zervou, P. Roumelioti, J.M. Matsoukas, R. Weisemann, An effort to understand the molecular basis of hypertension through the study of conformational analysis of losartan and sarmesin using a combination of Nuclear Magnetic Resonance spectroscopy and theoretical calculations, J. Med. Chem. 42 (1999) 1714–1722.
[13] P. Zoumpoulakis, A. Zoga, P. Roumelioti, N. Giatas, S.G. Grdadolnik, E. Iliodromitis, D. Vlahakos, D. Kremastinos, J.M. Matsoukas, T. Mavromoustakos, Conformational and biological studies for a pair of novel synthetic AT1 antagonists. Stereoelectronic requirements for antihypertensive efficacy, J. Pharm. Biomed. Anal. 31 (2003) 833–844.
[14] P. Zoumpoulakis, A. Politi, S.G. Grdadolnik, J.M. Matsoukas, T. Mavromoustakos, Structure elucidation and conformational study of V8. A novel synthetic non peptide AT1 antagonist, J. Pharm. Biomed. Anal. 40 (2006) 1097–1104.
[15] T. Mavromoustakos, M. Zervou, P. Zoumpoulakis, I. Kyrikou, N.P. Benetis, L. Polevaya, P. Roumelioti, N. Giatas, A. Zoga, P.M. Minakakis, A. Kolocouris, D. Vlahakos, S.G. Grdadolnik, J.M. Matsoukas, Conformation and bioactivity. Design and discovery of novel antihypertensive drugs, Curr. Top. Med. Chem. 4 (2004) 385–401.
[16] T. Mavromoustakos, P. Zoumpoulakis, I. Kyrikou, A. Zoga, E. Siapi, M. Zervou, I. Daliani, D. Dimitriou, A. Pitsasa, C. Kamoutsis, P. Laggner, Efforts to understand the molecular basis of hypertension trough drug:membrane interactions, Curr. Top. Med. Chem. 4 (2004) 445–459.
[17] J.N. Cohn, G. Tognoni, A randomized trial of the angiotensin-receptor blocker valsartan in chronic heart failure, N. Engl. J. Med. 345 (2001) 1667–1675.
[18] A. Chiolero, M. Burnier, Pharmocology of valsartan, an angiotensin II receptor antagonist, Expert Opin. Invest. Drugs 7 (1998) 1915–1925.
[19] M. De Gasparo, S. Whitebread, Binding of valsartan to mammalian angiotensin AT1 receptors, Regul. Pept. 59 (1995) 503–511.
[20] P. Buhlmayer, P. Furret, L. Criscione, M. De Gasparo, S. Whitebread, T. Schildin, R. Lattmann, J. Wood, Valsartan, a potent orally active angiotensin II antagonist developed from structurally new aminoacid series, Bioorg. Med. Chem. Lett. 4 (1994) 29–34.
[21] Y. Furukawa, S. Kishimoto, K. Nishikawa, Hypotensive Imidazole-5-Acetic Acid Derivatives. U.S. Patent 4355040, (1982).
[22] P. Zoumpoulakis, I. Daliani, M. Zervou, I. Kyrikou, E. Siapi, G. Lamprinidis, E. Mikros, T. Mavromoustakos, Losartan's molecular basis of interaction with membranes and AT1 receptor, Chem. Phys. Lipids 125 (2003) 13–25.
[23] C. Fotakis, S. Gega, E. Siapi, C. Potamitis, K. Viras, P. Moutevelis-Minakakis, C.G. Kokotos, S. Durdagi, S. Golic Grdadolnik, B. Sartori, M. Rappolt, T. Mavromoustakos, Interactions at the bilayer interface and receptor site induced by the novel synthetic pyrrolidinone analog MMK3, Biochim. Biophys. Acta 1768 (2010) 422–432.
[24] L.G. Herbette, Pharmacokinetic and pharmacodynamic design of lipophilic drugs based on a structural model for drug-interactions with biological membranes, Pesticide Sc. 35 (1992) 363–368.
[25] H.S. Young, V. Skita, R.P. Mason, L.G. Herbette, Molecular-basis for the inhibition of 1, 4-dihydropyridine calcium-channel drugs binding to their receptors by a non-specific site interaction mechanism, Biophys. J. 61 (1992) 1244–1255.
[26] T. Mavromoustakos, D.P. Yang, A. Makriyannis, Small angle x-ray diffraction and differential scanning calorimetric studies on O-methyl-(−)-Δ8 tetrahydrocannabinol and its 5′ iodinated derivative in membrane bilayers, Biochim. Biophys. Acta 1237 (1995) 183–188.
[27] M. McIntyre, S.E. Gaffe, R.A. Michaluck, J.L. Reid, Losartan, an orally active angiotensin (AT1) receptor antagonist: a review of its efficacy and safety in essential hypertension, Pharmacol. Ther. 74 (1997) 181–194.

[28] F.A. Oliveira, R. Morgado, M.V. Lima, B.A. Mello, A. Hansen, G.G. Batrouni, Comment on "dynamical foundations of nonextensive statistical mechanics", Phys. Rev. Lett. 90 (2003) 218901.
[29] T.J. Netticadan, T.F. Ashavaid, K.G. Nair, Characterisation of the canine cardiac sarcolemma in experimental mzocardial ischemia, Indian J. Clin. Biochem. 12 (1997) 49–54.
[30] R. Koynova, M. Caffrey, Phases and phase transitions of the phosphatidylcholines, Biochim. Biophys. Acta 1376 (1998) 91–145.
[31] M.D. Housley, K.K. Stanley, Dynamics of Biological Membranes, John Wiley and Sons, New York, 1982.
[32] I.W. Levin, R.N. Lewis, Fourier transform Raman spectroscopy of biological materials, Anal. Chem. 62 (1990) 1101A–1111A.
[33] J.C. Huang, J.R. Lapides, I.W. Levin, Phase-transition behaviour of saturated, symmetric chain phospholipid bilayers dispersions determined by Raman spectroscopy: correlation between spectral and thermodynamic parameters, J. Am. Chem. Soc. 104 (1982) 5926–5930.
[34] M. Rappolt, G. Pabst, Flexibility and structure of fluid bilayer interfaces, in: K. Nag (Ed.), Structure and dynamics of membranous interfaces, John Wiley & Sons, Hoboken, 2008, pp. 45–81.
[35] G. Pabst, H. Amenitsch, D.P. Kharakoz, P. Laggner, M. Rappolt, Structure and fluctuations of phosphatidylcholines in the vicinity of the main phase transition, Phys. Rev. E 70 (2004), 021908-1-021908-9.
[36] H. Amenitsch, M. Rappolt, M. Kriechbaum, H. Mio, P. Laggner, S. Bernstorff, First performance assessment of the small-angle X-ray scattering beamline at ELETTRA, J. Synchrotron Rad. 5 (1998) 506–508.
[37] G. Pabst, M. Rappolt, H. Amenitsch, P. Laggner, Structural information from multilamellar liposomes at full hydration: full q-range fitting with high quality x-ray data, Phys. Rev. E 62 (2000) 4000–4009.
[38] G. Pabst, J. Katsaras, V.A. Raghunathan, M. Rappolt, Structure and interactions in the anomalous swelling regime of phospholipid bilayers, Langmuir 19 (2003) 1716–1722.
[39] G. Pabst, Global properties of biomimetic membranes: perspectives on molecular features, Biophys. Rev. Lett. 1 (2006) 57–84.
[40] M. Rappolt, Bilayer thickness estimations with "poor" diffraction data, J. Appl. Phys. 107 (2010), art. no. 084701.
[41] J.F. Nagle, S. Tristram-Nagle, Structure and interactions of lipid bilayer: role of fluctuations, in: J. Katsaras, T. Gutberlet (Eds.), Lipid bilayers. Structure and interactions, Springer, Berlin, 2000, pp. 1–23.
[42] J.F. Nagle, S. Tristram-Nagle, Structure of lipid bilayers, Biochim. Biophys. Acta 1469 (2000) 159–195.
[43] S.W. Chiu, E. Jakobsson, R.J. Mashl, H.L. Scott, Cholesterol-induced modifications in lipid bilayers: a simulation study, Biophys. J. 83 (2002) 1842–1853.
[44] A. Hodzic, M. Rappolt, H. Amenitsch, G. Pabst, Differential modulation of membrane structure and fluctuations by plant sterols and cholesterol, Biophys. J. 94 (2008) 3935–3944.
[45] A.I. Greenwood, S. Tristram-Nagle, J.F. Nagle, Partial molecular volumes of lipids and cholesterol, Chem. Phys. Lipids 143 (2006) 1–10.
[46] E. Marti, H.R. Oswald, P. Bühlmyer, W. Marterer, Valsartan salts, European Patent Bulletin EP1313714B1 (2008).
[47] N. Albon, J.M. Sturtevant, Nature of the gel to liquid crystal transition of synthetic phosphatidylcholines, Proc. Natl. Acad. Sci. USA 75 (1978) 2258–2260.
[48] S. Tristram-Nagle, R. Zhang, R.M. Suter, C.R. Worthington, W.J. Sun, J.F. Nagle, Measurement of chain tilt angle in fully hydrated bilayers of gel phase lecithins, Biophys. J. 64 (1993) 1097–1109.
[49] J. Katsaras, S. Tristram-Nagle, Y. Liu, R.L. Headrick, E. Fontes, P.C. Mason, J.F. Nagle, Clarification of the ripple phase of lecithin bilayers using fully hydrated, aligned samples, Phys. Rev. E 61 (2000) 5668–5677.
[50] R.C. Spiker, I.W. Levin, Raman spectra and vibrational assignments for dipalmitoyl phosphatidylcholine and structurally related molecules, Biochim. Biophys. Acta 388 (1975) 361–373.
[51] N. Yellin, I.W. Levin, Hydrocarbon chain disorder in lipid bilayers: temperature dependent Raman spectra of 1, 2-diacyl phosphatidylcholine-water gels, Biochim. Biophys. Acta 489 (1977) 177–190.
[52] N. Yellin, I.W. Levin, Hydrocarbon chain trans-gauche isomerization in phospholipid bilayer gel assemblies, Biochemistry 16 (1977) 642–647.
[53] C.B. Fox, R.H. Uibel, J.M. Harris, Detecting phase transitions in phosphatidylcholine vesicles by Raman microscopy and self-modeling curve resolution, J. Phys. Chem. B 111 (2007) 11428–11436.
[54] T.J. O'Leary, P.D. Ross, I.W. Levin, Effects of anesthetic and nonanesthetic steroids on dipalmitoylphosphatidylcholine liposomes: a calorimetric and Raman spectroscopic investigation, Biochemistry 23 (1984) 4636–4641.
[55] N.B. Colthulp, L.H. Daly, S.E. Wiberley, Introduction to Infrared and Raman Spectroscopy, Academic Press, 1990.
[56] R.K. Bista, R.F. Bruch, A.M. Covington, Variable-temperature Raman spectromicroscopy for a comprehensive analysis of the conformational order in PEGylated lipids, J. RamanSpectrosc. 40 (2008) 463–471.
[57] T.J. O'Leary, I.W. Levin, Raman spectrosopic study of an interdigitated lipid bilayer diplamitoylphosphatidylcholine dispersed in glycerol, Biochim. Biophys. Acta 776 (1984) 185–189.
[58] J.R. Silvius, M. Lyons, P.L. Yeagle, T.J. O'Leary, Thermotropic properties of bilyers containing blanched-chain phospholipids, calorimetric, Raman and 31P NMR studies, Biochemistry 24 (1985) 5388–5395.
[59] M. Rappolt, G. Rapp, Structure of the stable and metastable ripple phase of dipalmitoylphosphatidylcholine, Eur. Biophys. J. 24 (1996) 381–386.
[60] R. Hosemann, S.N. Bagchi, Direct Analysis of Diffraction by Matter, North-Holland Publ. Co., Amsterdam, 1962.
[61] A. Caillé, Remarques sur la diffusion des rayons X dans les smectiques A, C. R. Acad. Sc. Paris B 274 (1972) 891–893.
[62] R. Zhang, S. Tristram-Nagle, W. Sun, R.L. Headrick, T.C. Irving, R.M. Suter, J.F. Nagle, Small-angle x-ray scattering from lipid bilayers is well described by modified Caillé theory but not by paracrystalline theory, Biophys. J. 70 (1996) 349–357.
[63] A. Seelig, J. Seelig, The dynamic structure of fatty acyl chains in a phospholipid bilayer measured by deuterium magnetic resonance, Biochemistry 13 (1974) 4839–4845.
[64] J.F. Nagle, D.A. Wilkinson, Lecithin bilayers. Density measurements and molecular interactions, Biophys. J. 23 (1978) 159–175.
[65] D.A. Wilkinson, J.F. Nagle, Dilatometry and calorimetry of saturated phosphatidylethanolamine dispersions, Biochemistry 20 (1981) 187–192.
[66] W.J. Sun, S. Tristram-Nagle, R.M. Suter, J.F. Nagle, Structure of the ripple phase in lecithin bilayers, Proc. Natl. Acad. Sci. USA 93 (1996) 7008–7012.
[67] M. Rappolt, G. Pabst, G. Rapp, M. Kriechbaum, H. Amenitsch, C. Krenn, S. Bernstorff, P. Laggner, New evidence for gel-liquid crystalline phase coexistence in the ripple phase of phosphatidylcholines, Eur. Biophys. J. 29 (2000) 125–133.
[68] R.J. Wittebort, C.F. Schmidt, R.G. Griffin, Solid-state carbon-13 nuclear magnetic resonance of the lecithin gel to liquid-crystalline phase transition, Biochemistry 20 (1981) 4223–4228.
[69] K. Pressl, K. Jørgensen, P. Laggner, Characterization of the sub-main-transition in distearoylphosphatidylcholine studied by simultaneous small- and wide-angle X-ray diffraction, Biochim. Biophys. Acta 1325 (1997) 1–7.
[70] K. Jørgensen, Calorimetric detection of a sub-main transition in long-chain phosphatidylcholine lipid bilayers, Biochim. Biophys. Acta 1240 (1995) 111–114.
[71] K.A. Riske, R.P. Barroso, C.C. Vequi-Suplicy, R. Germano, V.B. Henriques, M.T. Lamy, Lipid bilayer pre-transition as the beginning of the melting process, Biochim. Biophys. Acta 1788 (2009) 954–963.
[72] T. Heimburg, A model for the lipid pretransition: coupling of ripple formation with the chain-melting transition, Biophys. J. 78 (2000) 1154–1165.
[73] K. Sengupta, V.A. Raghunathan, J. Katsaras, Novel structural features of the ripple phase of phospholipids, Europhys. Lett. 49 (2000) 722–728.
[74] T.P. McMullen, R.N. McElhaney, New aspects of the interaction of cholesterol with dipalmitoylphosphatidylcholine bilayers as revealed by high-sensitivity differential scanning calorimetry, Biochim. Biophys. Acta 1234 (1995) 90–98.
[75] M.R. Vist, J.H. Davis, Phase equilibria of cholesterol/dipalmitoylphosphatidylcholine mixtures: 2 H nuclear magnetic resonance and differential scanning calorimetry, Biochemistry 29 (1990) 451–464.
[76] C. Fotakis, D. Christodouleas, P. Chatzigeorgiou, M. Zervou, N.-P. Benetis, K. Viras, T. Mavromoustakos, Development of a CP 31P NMR broadline simulation methodology for studying the interactions of antihypertensive AT1 antagonist losartan with phospholipid bilayers, Biophys. J. 96 (2009) 2227–2236.
[77] E. Theodoropoulou, D. Marsh, Interactions of angiotensin II non-peptide AT1 antagonist losartan with phospholipid membranes studied by combined use of di¡erential scanning calorimetry and electron spin resonance spectroscopy, Biochim. Biophys. Acta 1461 (1999) 135–146.
[78] E.S. Rowe, T.A. Cutrera, Differential scanning calorimetric studies of ethanol interactions with distearoylphosphatidylcholine: transition to the interdigitated phase, Biochemistry 29 (1990) 10398–10404.
[79] I.W. Levin, T.E. Thompson, Y. Barenholz, C. Huang, Two types of hydrocarbon chain interdigitation in sphingomyelin bilayers, Biochemistry 24 (1985) 6282–6286.
[80] G.S. Smith, E.B. Sirota, C.R. Safinya, N.A. Clark, Structure of the L beta phases in a hydrated phosphatidylcholine multimembrane, Phys. Rev. Lett. 60 (1988) 813–816.
[81] W.J. Sun, R.M. Suter, M.A. Knewtson, C.R. Worthington, S. Tristram-Nagle, R. Zhang, J.F. Nagle, Order and disorder in fully hydrated unoriented bilayers of gel phase dipalmitoylphosphatidylcholine, Phys. Rev. E 49 (1994) 4665–4676.
[82] E. Sevcsik, G. Pabst, A. Jilek, K. Lohner, How lipids influence the mode of action of membrane-active peptides, Biochim. Biophys. Acta 1768 (2007) 2586–2595.
[83] S. Danner, G. Pabst, K. Lohner, A. Hickel, Structure and thermotropic behavior of the Staphylococcus aureus lipid lysyl-dipalmitoylphosphatidylglycerol, Biophys. J. 94 (2008) 2150–2159.
[84] V.A. Parsegian, R.P. Rand, Interaction in membrane assemblies, in: R. Lipowsky, E. Sackmann (Eds.), Structure and Dynamics of Membranes, North-Holland, Amsterdam, 1995, pp. 643–690.
[85] G. Cevc, Membrane electrostatics, Biochim. Biophys. Acta 1031 (1990) 311–382.
[86] E. Cagigal, L. Gonzalez, R.M. Alonso, R.M. Jimenez, pKa determinination of angiotensin II receptor antagonists (ARA II) by spectrofluorimetry, J. Pharm. Biomed. Anal. 26 (2001) 477–486.
[87] M. Rappolt, M.F. Vidal, M. Kriechbaum, M. Steinhart, H. Amenitsch, S. Bernstorff, P. Laggner, Structural, dynamic and mechanical properties of POPC at low cholesterol concentration studied in pressure/temperature space, Eur. Biophys. J. 31 (2003) 575–585.
[88] H.I. Petrache, N. Gouliaev, S. Tristram-Nagle, R.T. Zhang, R.M. Suter, J.F. Nagle, Interbilayer interactions from high-resolution x-ray scattering, Phys. Rev. E 57 (1998) 7014–7024.